Application of Dynamic Sensitivity Theory to Assess the Thyristor-Based FACTS Controllers' Effect on the Transient Stability of Power Systems

E.A. Zamora-Cárdenas, C. R. Fuerte-Esquivel, L. Contreras-Aguilar

Abstract— **This paper describes the application of the dynamic sensitivity theory to assess the condition of stability of an electric power system subjected to a large perturbation. A unified power system transient stability study, including dynamic sensitivities, is described in detail. These sensitivities are derived for both a set of ordinary differential equations and differential-algebraic equations with respect to parameter variations. This theory is extended to consider Flexible AC Transmission System (FACTS) controllers in order to assess their impact on the power system dynamic trajectories due to large perturbations, as well as the controllers' capacity to extend the system's stable state-space region after the system is subjected to a disturbance. The FACTS controllers considered in this paper are the Static VARs Compensator (SVC) and Thyristor Controlled Series Compensator (TCSC). Results are reported in order to show the progress of the developed mathematical models and software.**

Index Terms—**Dynamic Sensitivities, Transient Stability, FACTS, power system security.**

I. Introduction

Transient stability analysis is one of the essential studies in the operation and planning of electric power system [1]. If this study determines that a rotor angle transient instability takes place due to large electromechanical oscillations among generation units and lack of synchronizing torque on the system, control actions need to be taken to prevent partial or complete service interruption. Among different preventive control measures whose application depends on the system operating condition, it is possible to applied compensation to regain an acceptable state of equilibrium after the disturbance [1]. Hence, the improvement of transient stability can be considered as a problem of controlling transient trajectories by change in parameters. Advances in Flexible AC Transmission Systems (FACTS) controllers have led to their application in improving stability of power networks [2]. The main idea behind FACTS is to use network parameters as controls to redirect power flow, as well as inject reactive power to the system, increasing the transient stability margin of power systems. In this context, assessment of system's transient stability condition is essential to quantify the effect of FACTS controllers' application. The stability condition can be computed by a time domain simulation which is applicable for arbitrarily complicated models, and it is feasible for large-scale power system analysis. However, this simulation only provides information about a single scenario, and repeated simulations have to be done to assess a degree of system's stability or instability.

Trajectory sensitivity (TS) analysis overcomes the need of repetitive simulation. In this approach, a linearization is carried out around a nominal trajectory rather than around an equilibrium point, such that it is possible to assess variations in the nominal transient trajectory resulting from perturbations in the underlying parameters and/or initial conditions [3]. These dynamic sensitivities provide a qualitative measure of how stable or instable a particular case may be, and valuable insights into the influence of parameters on the nominal transient trajectory of the system [3]. These capabilities of TS analysis are used in this paper to study the effect of FACTS controllers on the transient stability after the system is subjected to a disturbance. The system under consideration is the three-machine, nine-bus WSCC system [1]. Two FACTS controllers are considered in this paper, namely Static Var Compensator (SVC) and Thyristor Controller Series Compensation (TCSC), whose effectiveness is evaluated by carrying out a TS analysis with and without considering these controllers embedded in the system. The remainder of the paper is structured as follows: Section II describes a general differential-algebraic equations (DAE) model for a power system. Section III explains the derivation of the basic theory of TS analysis for DAEs form of the power system. Numerical examples are given in Section IV. Conclusions are drawn in Section V.

II. Power System Modeling

An electric power system can be represented by a set of parameter dependent differential equations constrained by a set of algebraic equations (DAEs), as given by (1).

$$\begin{aligned} \dot{x} &= f(x,y,\beta) \qquad f:\Re^{n+m+p}\to\Re^{n} \\ 0 &= g(x,y,\beta) \qquad g:\Re^{n+m+p}\to\Re^{m} \\ x\in X\subset\Re^{n} &\quad y\in Y\subset\Re^{m} \quad \beta\in B\subset\Re^{p} \end{aligned} \tag{1}$$

where x is a vector of dynamic state variables, y is a vector of instantaneous state, or algebraic, variables (usually complex node voltages); and β is a set of non-time varying system parameters. Due to the fact that transmission network dynamics are much faster than dynamics of the equipment or loads; it is considered that the variables y change

This work was supported by CONACyT, Mexico under the scholarship 169415.

Enrique A. Zamora-Cardenas, Claudio R. Fuerte-Esquivel, and Luis Contreras-Aguilar are with the Electrical Engineering Faculty, Universidad Michoacana de San Nicolás de Hidalgo (UMSNH), Morelia, Michoacan, 58000, Mexico (email:cfuerte@umich.mx). The first author is also with the Instituto Tecnológico Superior de Irapuato, at Guanajuato, México.

instantaneously with variations of the *x* states. Hence, only the dynamics of the equipment, e.g. generators, controls, FACTS devices, and load at buses, are explicitly modeled by the set of differential equations (1). The set of algebraic equations express the mismatch power flow equations at each node. As the power system can be viewed as an interconnection of several electric power plant components, particulars of each model are given below. All variables are given in per unit, unless it is specified otherwise.

A. Generator

In this paper, a classical generator model as described in [1] is considered, where the i^{th} machine is represented by a constant internal voltage source E_i behind the transient reactance X_{di} of the machine. The rotor mechanical model is given by the swing equations,

$$\begin{aligned} \dot{\delta}_i &= \omega_1 s_i \\ \dot{s}_i &= \frac{-D_i s_i + P_{Mi} - P_{gei}}{M_i} \\ s_i &= \frac{\omega_i - \omega_1}{\omega_1} \end{aligned} \tag{2}$$

where M_i is the moment of inertia in sec., D_i is the damping constant, P_{Gei} is the generator's electrical power output, P_{Mi} is the turbine mechanical power injection, δ_i is the generator's rotor angle in rad, ω_1 is the reference speed in rad/seg, ω_i is the actual rotor speed in rad/seg, and s_i is the generator slip. The ouput active power measured at generator's terminals is,

$$P_{gei} = \frac{E_i V_j}{X_{di}} \sin\left(\delta_i - \theta_j\right) \tag{3}$$

where V_j and θ_j are the magnitude and phase angle voltages at the j^{th} network node.

B. Network

This model consists of those equations expressing the active and reactive power balances at every system nodes. For the transmission element connected between nodes *i* and *j*, the active and reactive powers at the i^{th} node are,

$$\begin{aligned} P_{ij} &= V_i^2 G_{ii} + V_i V_j (G_{ij} \cos(\theta_i - \theta_j) + B_{ij} sin(\theta_i - \theta_j)) \\ Q_{ij} &= -V_i^2 B_{ii} + V_i V_j (G_{ij} sin(\theta_i - \theta_j) - B_{ij} \cos(\theta_i - \theta_j)) \end{aligned} \tag{4}$$

where V_j and θ_j are the voltages magnitude and phase angle at network nodes, $j = 1,\ldots,n_g + n_{PQ}$; respectively, and $\vec{Y}_{ij} = G_{ij} + jB_{ij}$ is the admittance of the transmission element connected between nodes *i* and *j*.

Assuming n_g generator nodes and n_{PQ} nodes with no generation, the mismatch power equations at the network nodes are,

$$\begin{aligned} P_{gei} &= P_{Li} + \sum_{j\in\Omega_i} P_{ij} \qquad \forall i = 1,\ldots,n_g \\ Q_{gei} &= Q_{Li} + \sum_{j\in\Omega_i} Q_{ij} \qquad \forall i = 1,\ldots,n_g \\ 0 &= P_{Li} + \sum_{j\in\Omega_i} P_{ij} \qquad \forall i = 1,\ldots,n_{PQ} \\ 0 &= Q_{Li} + \sum_{j\in\Omega_i} Q_{ij} \qquad \forall i = 1,\ldots,n_{PQ} \end{aligned} \tag{5}$$

where $\Omega_i = \{j : j \neq i\}$ is the set of nodes adjacent to *i*, and P_{Li} (Q_{Li}) is the active (reactive) power demanded by the load embedded at the i^{th} node.

If loads are modeled as constant impedances, the network can be reduced to the internal generator nodes. The algebraic equations are eliminated and the system can be described by a set of differential equations as follows,

$$\begin{aligned} M_i \ddot{\delta}_i + D_i \dot{\delta}_i = P_{Mi} - E_i^2 G_{ii} \\ - \sum_{\substack{j=1 \\ j\neq i}}^{n_g} \left(C_{ij} \sin\left(\delta_i - \delta_j\right) + D_{ij} \cos\left(\delta_i - \delta_j\right) \right) \end{aligned} \tag{6}$$

where $C_{ij} = E_i E_j B_{ij}$ and $D_{ij} = E_i E_j G_{ij}$. $\vec{Y}_{ij} = G_{ij} + jB_{ij}$ is an element of the nodal admittance matrix of the reduced system.

C. Static Var Compensator.

An SVC can be considered as a variable shunt reactance which is adjusted in response to power system operative conditions in order to control specific parameters of the network. This adjustment is carried out by the firing angle of the thyristors via a proportional-integral controller. Depending on the equivalent SVC's reactance, i.e. capacitive or inductive, the SVC is capable of drawing capacitive or inductive current from the electric power system at their coupling point. Suitable control of this equivalent reactance allows the regulation of the voltage magnitude at the power system node where the SVC is connected. Figure 1 shows the block diagram representing the dynamic operation of this controller [4,5].

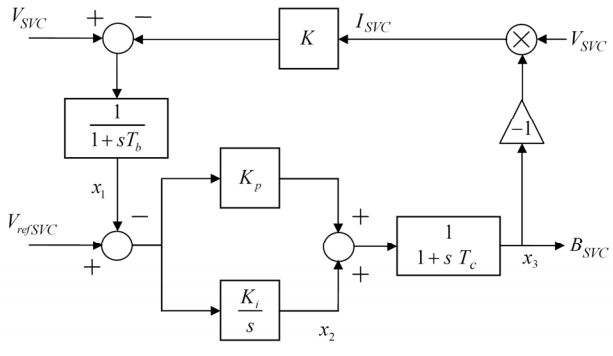

Fig. 1. SVC block diagram.

The SVC admittance seen by the system is the state variable B_{SVC}. Based on this block diagram, it is possible to derive the set of DAEs given in eq. (7) [5].

$$
\begin{aligned}
\dot{x}_1 &= \frac{1}{T_b}\left(V_{SVC}(1+KB_{SVC}) - x_1\right) \\
\dot{x}_2 &= K_i\left(V_{ref.SVC} - x_1\right) \\
\dot{B}_{SVC} &= \frac{1}{T_c}\left(x_2 + K_p(V_{ref.SVC} - x_1) - B_{SVC}\right) \\
Q_{SVC} &= V_{SVC}^2 B_{SVC}
\end{aligned}
\tag{7}
$$

D. Thyristor Controlled Series Compensation.

One important FACTS component is the TCSC which allows rapid and continuous change of the transmission line apparent impedance. The control scheme used for this device depends on the purpose of its installation. The constant current control regulates the current magnitude through the compensated line at a desired value by suitably varying the TCSC's reactance [6]. As a result of this control, the active power flowing along the compensated transmission line can be maintained at a specified value under a range of different scenarios of operative conditions. On the other hand, the constant angle control regulates the voltage drop across the compensated line, which will help to damp power angle oscillations in the system [7]. The block diagram shown in Fig. 2 can be used to represent both control schemes.

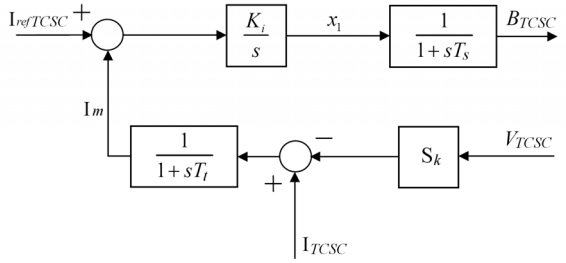

Fig. 2. TCSC block diagram.

The sensed current is given by $I_m = I_{TCSC} - S_k V_{TCSC}$, where V_{TCSC} is the voltage across the controller. If S_k is set equal to zero, the constant current control is achieved. If S_k is set equal to the slope $-1/X_L$, where X_L is the compensated line reactance, the constant angle control is achieved [7]. A change in the thyristor's firing angle results from the integration of the current error signal given by $I_{refTCSC} - I_m$, such that the TCSC's reactance is modulated. T_s represents the delay time associated to the thyristor controller action whilst T_t represents the transducer time constant. The state equations of the TCSC connected between nodes *i* and *j* are given by (8).

III. Dynamic Sensitivity Theory

The dynamic sensitivity (also called trajectory sensitivity) theory with respect to (w.r.t.) changes in parameters is presented in this section.

$$
\begin{aligned}
\dot{I}_m &= \frac{1}{T_t}\left[\sqrt{V_i^2 + V_j^2 - 2V_iV_j\cos(\theta_i - \theta_j)}\left(\frac{1}{|X_{TCSC}|} - S_k\right) - I_m\right] \\
\dot{x}_1 &= K_1(I_{refTCSC} - I_m) \\
\dot{X}_{TCSC} &= \frac{1}{T_s}(x_1 - X_{TCSC})
\end{aligned}
\tag{8}
$$

A. Dynamic sensitivity theory for ODEs

The following theoretical treatment to obtain dynamic sensitivities for ordinary differential equations (ODEs) is described in detail in [8], based on an *n*-dimensional nonlinear dynamic system $f(t, x(t,\beta), \beta)$ which is continuous in $(t, x(t,\beta), \beta)$ and has continuous first partial derivatives w.r.t. $x(t,\beta)$ and β for all $(t, x(t,\beta), \beta) \in [t_0, t_1] \mathrm{x} \Re^n \mathrm{x} \Re^p$.

Let β_0 be the nominal value of β, and assume the nominal state equation $\dot{x} = f(t, x(t,\beta), \beta_0)$, $x(t_0, \beta_0) = x_0$ has a unique nominal trajectory solution $x(t, \beta_0)$ over $[t_0, t_1]$. The sensitivities of the state trajectories with respect to system parameters can be found by perturbing β from its nominal value β_0. Then, for all β sufficiently close to β_0, the state equation $\dot{x} = f(t, x(t,\beta), \beta)$, $x(t_0, \beta) = x_0$ has a unique perturbed trajectory solution $x(t,\beta)$ over $[t_0, t_1]$ that is close to the nominal trajectory solution $x(t, \beta_0)$. This perturbed solution is given by,

$$
x(t,\beta) = x_0 + \int_{t_0}^{t} f\left(s, x(s,\beta), \beta\right) ds \tag{9}
$$

The continuous differentiability of $f(\cdot)$ w.r.t. x and β implies that (9) is differentiable w.r.t. β near β_0. Since x_0 is independent of β, this partial derivative is,

$$
\frac{\partial x(t,\beta)}{\partial \beta} = \int_{t_0}^{t}\left[\frac{\partial f\left(s, x(s,\beta), \beta\right)}{\partial x(s,\beta)}\frac{\partial x(s,\beta)}{\partial \beta} + \frac{\partial f\left(s, x(s,\beta), \beta\right)}{\partial \beta}\right] ds \tag{10}
$$

In this case, the sensitivity of the trajectories of *x* w.r.t. β (also called sensitivity function) is defined as (11), which is a matrix of order *nxp*.

$$
x_\beta = \left[\frac{\partial x(t,\beta)}{\partial \beta}\right] \tag{11}
$$

Differentiating (10) w.r.t. *t*, it can be demonstrated that x_β satisfies the differential equation,

$$
\dot{x}_\beta = A(t,\beta)x_\beta + B(t,\beta), \quad x_\beta(t_0, \beta) = 0 \tag{12}
$$

where,

$$
\begin{aligned}
A(t,\beta) &= \left.\frac{\partial f\left(s, x(s,\beta), \beta\right)}{\partial x(s,\beta)}\right|_{x = x(s,\beta)} \\
B(t,\beta) &= \left.\frac{\partial f\left(s, x(s,\beta), \beta\right)}{\partial \beta}\right|_{x = x(s,\beta)}
\end{aligned}
\tag{13}
$$

Based on the described procedure, an approach for calculating x_β consists of appending the differential equation (12) with the nominal state equation to obtain the (n+np) set of ODEs given by,

$$\begin{aligned} \dot{x} &= f\left(t, x(t,\beta), \beta_0\right), & x(t_0) &= x_0 \\ \dot{x}_\beta &= A\left(t,\beta\right)x_\beta + B\left(t,\beta\right), & x_\beta\left(t_0\right) &= 0 \end{aligned} \tag{14}$$

which is solved numerically at the nominal value β_0 for the nominal solution and the sensitivity function simultaneously.

B. *Dynamic sensitivity theory for DAEs*

In the context of power systems, this theory can be apply to DAEs to find out how sensitive the trajectories of each state are to variations in system parameters, providing a measurement of system security. A multi-machine power system is modeled by a set of DAEs as given by (1), which can be expressed as a function of the perturbed solution (9) as follows,

$$\begin{aligned} x(t,\beta) &= x_0 + \int_{t_0}^{t} f(x,y,\beta)ds \\ 0 &= g(x,y,\beta) \end{aligned} \tag{15}$$

The sensitivities of each state vector to chosen system parameter, $x_\beta = \partial x/\partial\beta$ and $y_\beta = \partial y/\partial\beta$, are obtained from the partial derivative of (15) w.r.t. β,

$$\begin{aligned} \frac{\partial x}{\partial\beta} &= \int_{t_0}^{t}\left(\frac{\partial f(\cdot)}{\partial x}\frac{\partial x}{\partial\beta} + \frac{\partial f(\cdot)}{\partial y}\frac{\partial y}{\partial\beta} + \frac{\partial f(\cdot)}{\partial\beta}\right)ds \\ 0 &= \frac{\partial g(\cdot)}{\partial x}\frac{\partial x}{\partial\beta} + \frac{\partial g(\cdot)}{\partial y}\frac{\partial y}{\partial\beta} + \frac{\partial g(\cdot)}{\partial\beta} \end{aligned} \tag{16}$$

Lastly, in order to obtain the trajectory of sensitivities, (16) is differentiating w.r.t. t,

$$\begin{aligned} \dot{x}_\beta &= \frac{\partial f(\cdot)}{\partial x}x_\beta + \frac{\partial f(\cdot)}{\partial y}y_\beta + \frac{\partial f(\cdot)}{\partial\beta} \quad , \; x_\beta(t_0) = 0 \\ 0 &= \frac{\partial g(\cdot)}{\partial x}x_\beta + \frac{\partial g(\cdot)}{\partial y}y_\beta + \frac{\partial g(\cdot)}{\partial\beta} \quad , \; y_\beta(t_0) = 0 \end{aligned} \tag{17}$$

Equations (1) and (17) are solved numerically at the nominal value β_0 for the nominal solution (x, y) and the sensitivity function (x_β, y_β) simultaneously.

A chart flow of the algorithm's solution is shown in Fig. 3. In this case, variables S_α^X and S_α^Y correspond to x_β and y_β, respectively.

IV. Study Cases

The assessment of FACTS controllers' effect on the transient stability based on the application of trajectory sensitivities is carried out by computing the sensitivity of the post-disturbance trajectory for a given clearing time t_{cl} with respect to a chosen parameter. As the t_{cl} increases, the peak of these sensitivities increases such that the system approaches to its boundary stable region of attraction. The WSCC three-machine, nine-bus system shown in Fig. 4 is examined with and without a FACTS controller considering sensitivities with respect to the modified mechanical input torque $P_i = P_{m\,i} - E_i^2 G_{ii}$ $i = 1,2,3$ only, $\beta = [P_1 \quad P_2 \quad P_3]^T$, due to the system stress is related to the scheduled generation. The system and controllers data are given in the Appendix. In order to assess the FACTS effect, the system disturbance consists in the connection of load at node 7, which is disconnected after a specified clearing time.

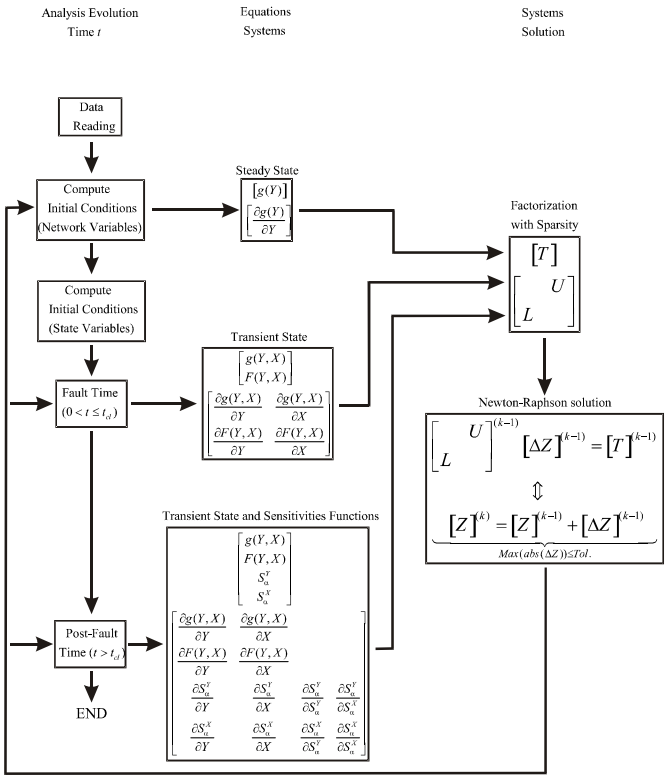

Fig. 3. Block diagram for transient sensitivity analysis.

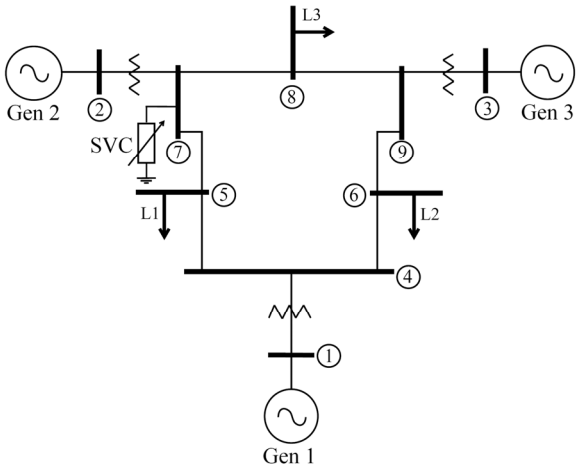

Fig. 4. WSCC system with an SVC.

A. *Effect of shunt compensation with SVC.*

A SVC is connected to the system as indicated at Fig. 4. A load of $P_{L7} = 0.3$ pu and $Q_{L7} = 0.9$ pu is connected at bus 7 to quantify the performance of the controller. The load is disconnected at different clearing times as indicate in Table I. The set of DAEs that represent the system are given by (2), (3), (5) and (7). The state vector is given by (18) and the sensitivity matrix is given by (19).

$$x = [\omega_1 \quad \omega_2 \quad \delta_2 \quad \omega_3 \quad \delta_3 \quad x_1 \quad x_2 \quad B_{SVC}] \qquad (18)$$

$$\frac{\partial x}{\partial \beta} = \begin{bmatrix} \frac{\partial \omega_1}{\partial P_1} & \frac{\partial \omega_2}{\partial P_1} & \frac{\partial \delta_2}{\partial P_1} & \frac{\partial \omega_3}{\partial P_1} & \frac{\partial \delta_3}{\partial P_1} & \frac{\partial x_1}{\partial P_1} & \frac{\partial x_2}{\partial P_1} & \frac{\partial B_{SVC}}{\partial P_1} \\ \frac{\partial \omega_1}{\partial P_2} & \frac{\partial \omega_2}{\partial P_2} & \frac{\partial \delta_2}{\partial P_2} & \frac{\partial \omega_3}{\partial P_2} & \frac{\partial \delta_3}{\partial P_2} & \frac{\partial x_1}{\partial P_2} & \frac{\partial x_2}{\partial P_2} & \frac{\partial B_{SVC}}{\partial P_2} \\ \frac{\partial \omega_1}{\partial P_3} & \frac{\partial \omega_2}{\partial P_3} & \frac{\partial \delta_2}{\partial P_3} & \frac{\partial \omega_3}{\partial P_3} & \frac{\partial \delta_3}{\partial P_3} & \frac{\partial x_1}{\partial P_3} & \frac{\partial x_2}{\partial P_3} & \frac{\partial B_{SVC}}{\partial P_3} \end{bmatrix}^T \qquad (19)$$

Table I shows the peak of the sensitivities of machines angles w.r.t. modified mechanical input torque with the controller disconnected and connected to the system.

TABLE I. COMPARISON OF MAXIMUM SENSITIVITIES WITH AND WITHOUT SVC FOR DIFFERENT CLEARING TIMES.

Sensitivity	Without SVC		With SVC	
	$\partial\delta_2/\partial P_2$	$\partial\delta_3/\partial_3$	$\partial\delta_2/\partial P_2$	$\partial\delta_3/\partial P_3$
t_{cl}=0.01 s.	11.7576	4.4756	11.6916	4.4558
t_{cl}=0.10 s.	23.5407	11.5781	16.1887	8.1623
t_{cl}=0.15 s.	201.8799	113.4272	22.7245	11.6837
t_{cl}=0.20 s.	Unstable	Unstable	35.8159	18.8781

The results shows that the peak values of sensitivities increases as the clearing time gets larger and the system becomes more in danger of losing synchronism. Because the sensitivity $\partial\delta_2/\partial P_2$ is larger in every case, machine two is more critical than machine three. Also, by comparing both cases at identical clearing times, it is observed that when the SVC is embedded in the system, the peak values of sensitivities do not increase as much as when the SVC is not included. This means that the SVC improves the transient stability of the system by adding reactive power during the disturbance. This statement is demonstrated in figs. 5 and 6.

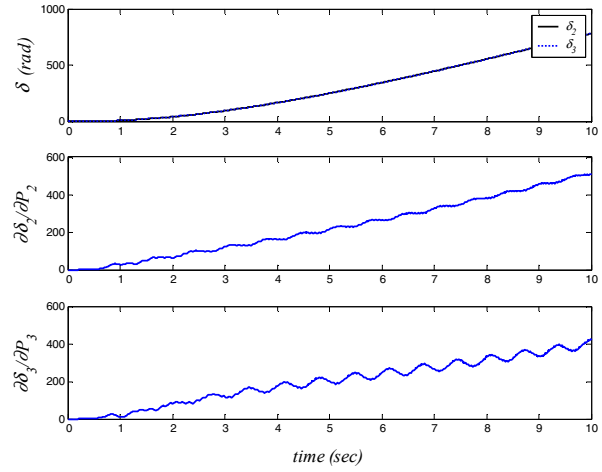

Fig. 5. Angles and sensitivities for t_{cl}=20 seconds without SVC.

Figure 5 shows the swing curves for the rotors angles of machines 2 and 3, as well as their respective sensitivities for a clearing time of 20 seconds when the SVC is not connected to the system. The same quantities are shown in Fig. 6 but with the SVC embedded to the system. The comparison of both set of results shows that when the SVC is connected to the system, the machine angles do not lose synchronism, and the SVC helps to damp the oscillations.

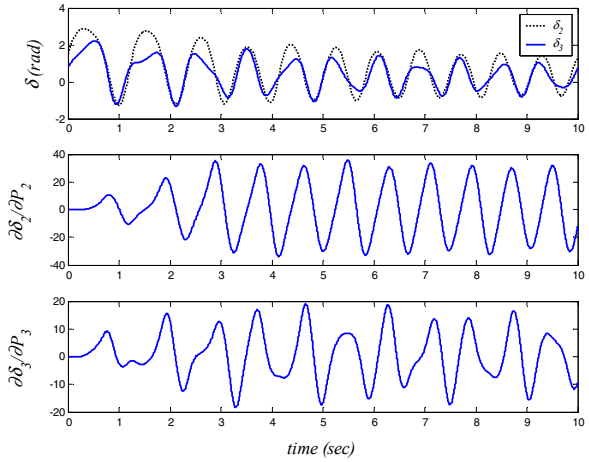

Fig. 6. Angles and sensitivities for t_{cl}=20 seconds with SVC.

Furthermore, the sensitivities values remain within limits, instead of having a continuous increment as a function of time. The reason for the higher sensitivity of P_2 is that the disturbance takes place in a node which is electrically closer to machine 2.

Figure 7 shows the SVC state variables as a function of time for the case under analysis. At the pre-disturbance operation state, the variable x_1 has a value equal to the voltage magnitude measured at the SVC node. During the disturbance period, this value decreases due to the increment of load and absorption of reactive power. Hence, the variables x_2 and B_{SVC} begin to rise to supply more reactive power to the system. Once the load is disconnected, the SVC return to their initial values.

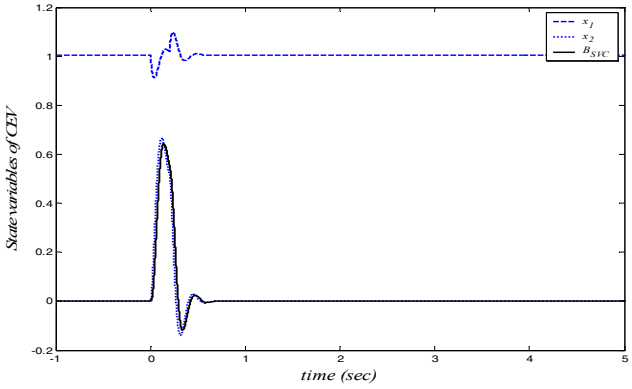

Fig. 7. SVC state variables.

Figure 8 shows the sensitivities of machine angles w.r.t. the SVC control gains. It is observed that the block K has the major impact on the system dynamic performance. This is because this block corresponds to the slope of the SVC control characteristic, which determines the amount of reactive power to be injected by the controller.

B. Effect of series compensation with TCSC.

A TCSC is connected to the system as indicated in Fig. 9 with parameters as indicated in the Appendix. Similarly to the disturbance applied in the last section, a load of $P_{L7} = 1.0$ pu and $Q_{L7} = 0.2$ pu is connected at bus 7 and after a certain period of time it is disconnected from the system.

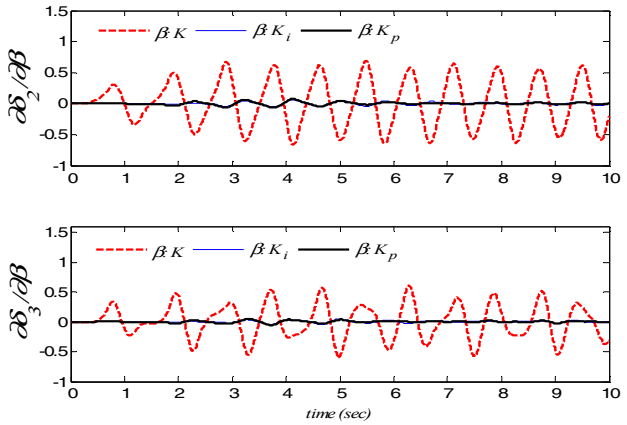

Fig. 8. Rotor angle sensitivities w.r.t. SVC control gains.

For the study of dynamic sensitivities, the results obtained with a TCSC connected in the system are compared with those obtained when a fixed series capacitor replaces the controller. In this case, the capacitor value corresponds to the TCSC's equivalent susceptance value when it is operating at the capacitive region in the pre-disturbance state. The set of equations (2), (3), (5) and (8) are used to represent the system with the TCSC. For the simulated case, the TCSC is operating in constant current mode control. Sensitivity results for different load clearing times are presented in Table II.

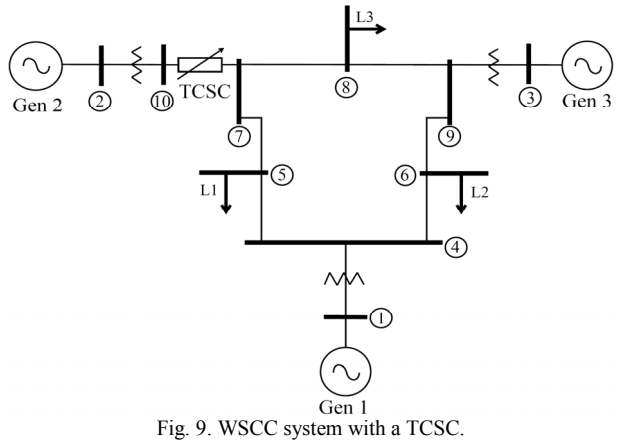

Fig. 9. WSCC system with a TCSC.

TABLE II. COMPARISON OF THA MAXIMUMS SENSITIVITIES OF THE SYSTEM WITH SERIES COMPENSATION

Sensitivity	With Fixed Capacitor		With TCSC	
	$\partial\delta_2/\partial P_2$	$\partial\delta_3/\partial P_3$	$\partial\delta_2/\partial P_2$	$\partial\delta_3/\partial P_3$
t_{cl}=0.01 s.	2.8972	0.5990	2.8775	0.5980
t_{cl}=0.10 s.	9.3752	0.8469	7.9871	0.7537
t_{cl}=0.15 s.	14.5048	1.1642	11.8364	0.9624
t_{cl}=0.20 s.	27.5641	1.9870	18.5321	1.3239
t_{cl}=0.25 s.	Unstable	11.4260	69.3096	4.6837

As observed in the last section, as the clearing time increases, the system approaches to its stability boundary, as indicated by the increment of the sensitivity peak value. Comparing results at identical clearing times, it is observed that the system is less stressed when the TCSC is connected in the system. For a clearing time of 0.25 seconds, the system loses synchronism when it is compensated with a fixed capacitor whilst the TCSC allows it to remain in synchronism. The observations based on the peak values of sensitivities are confirmed by analyzing the rotor angle profile of machines 2 and 3 as a function of time, for a clearing time of 0.25 seconds, showed in Fig. 10 and their sensitivities showed in Fig. 11.

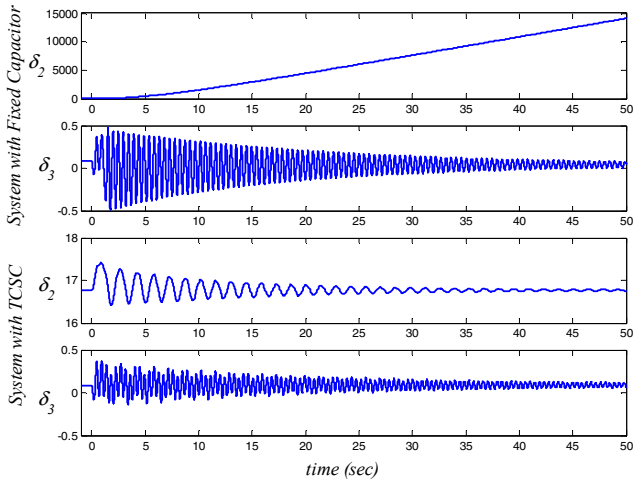

Fig. 10. Rotor angle profiles for t_{cl}=0.25 seconds with series compensation.

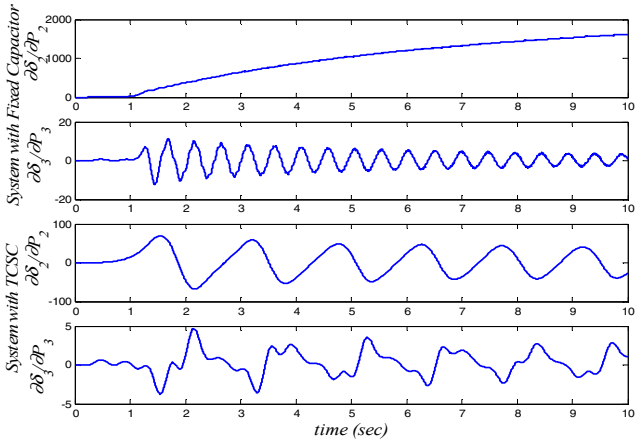

Fig. 11. Sensitivities for t_{cl}=0.25 seconds with series compensation.

The dynamic performance of the TCSC control variables is shown in Fig. 12. At the time of the disturbance, the TCSC current increases its value and the controller modulates its equivalent reactance in order to adjust the current at the nominal value. This adjustment takes place during the disturbance and post-disturbance operating periods until the original TCSC control variable values are obtained due to the system has returned to its original operating point. The sensitivities of machine angles w.r.t. the TCSC control gains are shown in Fig. 13. It is observed that rotor angles are very sensitive w.r.t. the variable s_k which determines the TCSC control operation mode.

V. CONCLUSIONS

This paper describes the application of the dynamic sensitivity theory to assess the effect of FACTS controllers on the transient stability condition of a power system. It has been observed that both SVC and TCSC helped to stabilize the system in a transient stability sense. This effect has been quantified based on the peak values of sensitivities, as they decrease for identical clearing time when the controller is embedded in the system. It was also shown how the machine variables changes w.r.t. the FACTS controller gains, such that it is possible to determine which control parameters have more effect on the system dynamics.

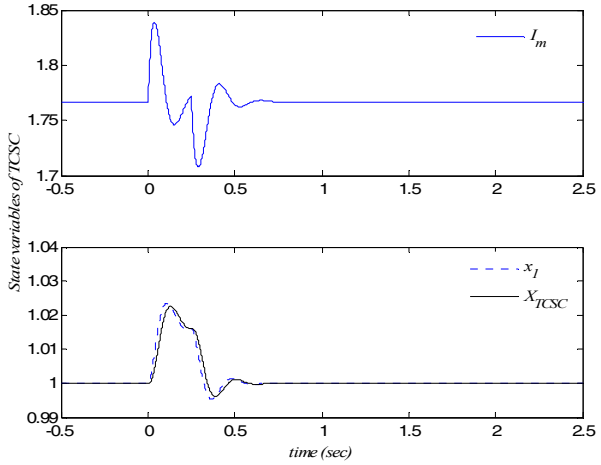

Fig. 12. TCSC state variables.

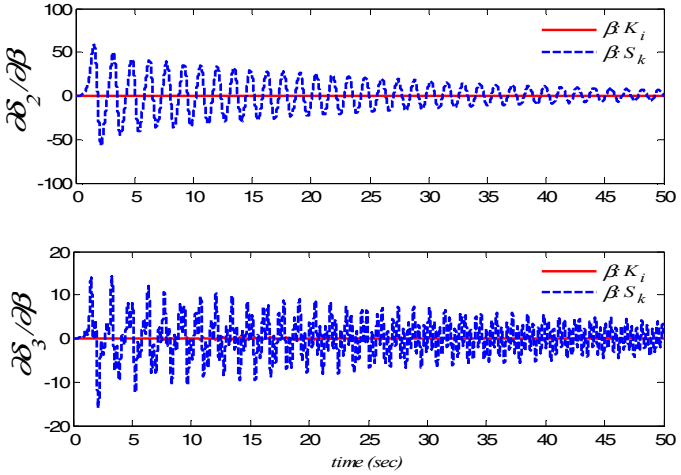

Fig. 13. Rotor angle sensitivities w.r.t. TCSC control gains.

APPENDIX

System and FACTS controllers data are given in the following tables.

TABLE III. SYSTEM LINE DATA

From node	*To node*	R	X_L	B_{TOTAL}
1	4		0.1184	
2	7		0.1823	
3	9		0.2399	
4	5	0.010	0.085	0.088
4	6	0.017	0.092	0.079
5	7	0.032	0.161	0.153
6	9	0.039	0.170	0.179
7	8	0.0085	0.072	0.0745
8	9	0.0119	0.1008	0.1045

TABLE IV. GENERATOR DATA

Node	x'_d	x'_q	τ'_{d0}	τ'_{q0}	H	D
1	0.0608	0.0969	8.96	0.31	23.64	0.01254
2	0.1198	0.1969	6.0	0.535	6.40	0.0068
2	0.1813	0.25	5.89	0.6	3.01	0.0048

TABLE V. SVC DATA

K	T_c	T_b	K_p	K_i
0.1	0.02	0.02	0.0	100

TABLE VI. TCSC DATA

K_i	T_s	T_t	S_k
5	0.02	0.02	0.0 ó -1/X_L

TABLE VII. LOAD DATA

Node	R_C	X_C
5	1.25	0.50
6	0.90	0.30
7	1.00	0.35

REFERENCES

[1] Kundur, P., *Power System Stability and Control*, McGraw Hill, 1994.

[2] Song Y.H. and Johns A.T. (Editors), *Flexible AC Transmission Systems (FACTS)*, IEE Power and Energy series 30, 1999.

[3] Laufenberg M. J. and Pai M. A., "A new approach to dynamic security assessment using trajectory sensitivities," IEEE Transactions on Power Systems, Vol. 13, No. 3, Aug. 1998, pp. 953-958 .

[4] Padiyar K.R. and Varma R.K., "Damping torque analysis of static var system controllers," IEEE Transactions on Power System, Vol. 6, No. 2, May 1991, pp. 458-465.

[5] Laufenberg M.J., Pai M.A. and Padiyar K.R., "Hopf bifurcation control in power systems with static var compensators," International Journal of Electrical Power and Energy Systems, Vol. 19, No. 5, June 1997, pp. 339-347.

[6] Christl N., Hedin R., Sadek K., Lützelberger P., Krause P.E., McKenna S.M., Montoya A.H. and Togerson D.: 'Advanced Series Compensation (ASC) with Thyristor Controlled Impedance', International Conference on Large High Voltage Electric Systems (CIGRÉ), paper 14/37/38-05, Paris, September 1992.

[7] Padiyar K.R., Geetha M.K. and Rao K.U., "A novel power flow controller for controlled series compensator," AC and DC Power Transmission Conference, 29 April-3, London England, May 1996, pp. 329-334.

[8] Khalil H.S., *Nonlinear systems*, Macmillan, 1992.

Enrique A. Zamora-Cardenas received the B.Eng. (Hons.) degree in 1999 from the University of Colima, Colima, México, and the MS degree in 2004 from the Universidad Michoacana de San Nicolás de Hidalgo (UMSNH), Morelia, México, in 2004. He is currently pursuing the PhD degree in UMSNH in the area of dynamic and steady-state analysis of FACTS. He is also an Associate Professor at the Instituto Tecnológico Superior of Irapuato, at Irapuato, Guanajuato, México.

Claudio R. Fuerte-Esquivel (M'91) received the B.Eng. (Hons.) degree from the Instituto Tecnológico de Morelia, Morelia, México, in 1990, the MS degree (*summa cum laude*) from the Instituto Politécnico Nacional, México, in 1993, and the PhD degree from the University of Glasgow, Glasgow, Scotland, U.K., in 1997. Currently, he is an Associate Professor at the Universidad Michoacana de San Nicolás de Hidalgo (UMSNH), Morelia, where his research interests lie in the dynamic and steady-state analysis of FACTS.

Luis Contreras-Aguilar received the B.Eng. (Hons.) degree in 2000 from the University of Colima, Colima, México, and the MS degree in 2005 from the Universidad Michoacana de San Nicolás de Hidalgo (UMSNH), Morelia, México, in 2004. He is currently pursuing the PhD degree in UMSNH in the area of power quality.